PeerJ Computer Science   Manuscript to be reviewed

Machine-learning-based automated quantification machine for virus plaque assay counting

Gridsada Phanomchoeng [Corresp., 1, 2] , **Chayatorn Kukiattikoon** [1] , **Suphanut Plengkham** [1] , **Siwaporn Boonyasuppayakorn** [2, 3] , **Saran Salakij** [1, 2] , **Suvit Poomrittigul** [4] , **Lunchakorn Wuttisittikulkij** [Corresp. 5]

[1] Department of Mechanical Engineering, Faculty of Engineering, Chulalongkorn University, Chulalongkorn University, Bangkok, 10330, Thailand

[2] Applied Medical Virology Research Unit, Chulalongkorn University, Chulalongkorn University, Bangkok, 10330, Thailand

[3] Department of Microbiology, Chulalongkorn University, Chulalongkorn University, Bangkok, 10330, Thailand

[4] Department of Software Engineering and Information System, Pathumwan Institute of Technology, Pathumwan Institute of Technology, Bangkok, 10330, Thailand

[5] Department of Electrical Engineering, Faculty of Engineering, Chulalongkorn University, Chulalongkorn University, Bangkok, 10330, Thailand

Corresponding Authors: Gridsada Phanomchoeng, Lunchakorn Wuttisittikulkij
Email address: gridsada.phanomchoeng@gmail.com, lunchakorn.w@chula.ac.th

The plaque assay is a standard quantification system in virology for verifying infectious particles. One of the complex steps of plaque assay is the counting of the number of viral plaques in multiwell plates to study and evaluate viruses. Manual counting plaques are time-consuming and subjective. There is a need to reduce the workload in plaque counting and for a machine to read virus plaque assay; thus, herein, we developed a machine-learning (ML)-based automated quantification machine for viral plaque counting. The machine consists of two major systems: hardware for image acquisition and ML-based software for image viral plaque counting. The hardware is relatively simple to set up, affordable, portable, and automatically acquires a single image or multiple images from a multiwell plate for users. For a 96-well plate, the machine could capture and display all images in less than 1 min. The software is implemented by K-mean clustering using ML and unsupervised learning algorithms to help users and reduce the number of setup parameters for counting and is evaluated using 96-well plates of dengue virus. Bland–Altman analysis indicates that more than 95% of the measurement error is in the upper and lower boundaries [±2 standard deviation]. Also, gage repeatability and reproducibility analysis showed that the machine is capable of applications. Moreover, the average correct measurements by the machine are 85.8%. The ML-based automated quantification machine effectively quantifies the number of viral plaques.

Machine-learning-based automated quantification machine for virus plaque assay counting

Gridsada Phanomchoeng[1,2], Chayatorn Kukiattikoon[1], Suphanut Plengkham[1], Siwaporn Boonyasuppayakorn[2,3], Saran Salakij[1,2], Suvit Poomrittigul[4], Lunchakorn Wuttisittikulkij[5]

[1] Department of Mechanical Engineering, Faculty of Engineering, Chulalongkorn University, Bangkok, 10330, Thailand
[2] Applied Medical Virology Research Unit, Chulalongkorn University, Bangkok 10330, Thailand
[3] Department of Microbiology, Chulalongkorn University, Bangkok 10330, Thailand
[4] Department of Software Engineering and Information System, Pathumwan Institute of Technology, Bangkok, 10330, Thailand.
[5] Department of Electrical Engineering, Faculty of Engineering, Chulalongkorn University, Bangkok, 10330, Thailand

Corresponding Author:
Lunchakorn Wuttisittikulkij[5]
Department of Electrical Engineering, Faculty of Engineering, Chulalongkorn University,
Bangkok, 10330, Thailand
Email address: lunchakorn.w@chula.ac.th
Gridsada Phanomchoeng[1,2]
Department of Mechanical Engineering, Faculty of Engineering, Chulalongkorn University,
Bangkok, 10330, Thailand
Email address: gridsada.p@chula.ac.th

Abstract

The plaque assay is a standard quantification system in virology for verifying infectious particles. One of the complex steps of plaque assay is the counting of the number of viral plaques in multiwell plates to study and evaluate viruses. Manual counting plaques are time-consuming and subjective. There is a need to reduce the workload in plaque counting and for a machine to read virus plaque assay; thus, herein, we developed a machine-learning (ML)-based automated quantification machine for viral plaque counting. The machine consists of two major systems: hardware for image acquisition and ML-based software for image viral plaque counting. The hardware is relatively simple to set up, affordable, portable, and automatically acquires a single image or multiple images from a multiwell plate for users. For a 96-well plate, the machine could capture and display all images in less than 1 min. The software is implemented by K-mean clustering using ML and unsupervised learning algorithms to help users and reduce the number of setup parameters for counting and is evaluated using 96-well plates of dengue virus. Bland–Altman analysis indicates that more than 95% of the measurement error is in the upper and lower boundaries [±2 standard deviation]. Also, gage repeatability and reproducibility analysis showed that the machine is capable of applications. Moreover, the average correct measurements by the machine are 85.8%. The ML-based automated quantification machine effectively quantifies the number of viral plaques.

Introduction

A plaque assay is one of the standard measurements (Dulbecco, 1952) for viable viruses in virology laboratories. Applications of this method range from basic research through drug discovery to vaccine development (Premsattham et al., 2019). In principle, viruses infect the cell monolayer in a semisolid medium, thus limiting only the horizontal spread. The area of cell death (i.e. plaque) is visualized under a microscope before staining with neutral red or crystal violet (BioTek Instruments, 2021; Cacciabue et al., 2019). The plate is manually counted and calculated to quantify the virus. The manual counting of plaques is tedious and requires well-trained personnel for verification. The plaque assay can be performed in low to medium throughput formats, such as 6-, 12-, or 24-well plates. This method requires more reagents and highly skilled operators to appropriately perform the assay. Recently, a simplified microwell plaque titration assay was developed with Herpes simplex (Bhattarakosol, Yoosook & Cross, 1990) and dengue viruses (Boonyasuppayakorn et al., 2016). Automated data acquisition and quantification methods have been developed under a flatbed scanner (Boonyasuppayakorn et al., 2016; Sullivan et al., 2012).

Recently, automated imaging-based counters have been applied to plaque assays; however, the current versions face multiple challenges. For example, Cellular Technology Limited developed a commercial Elispot and viral plaque-counting machine called ImmunoSpot CLT Analyzers (e.g. Cellular Technology Limited, 2021). The machines can automatically acquire high-resolution images for each well plate with a high speed and automatically count plaque using software. Even though the software focuses on counting Elispot assays the company can

65 optimize the setup, such as plaque intensity and size to develop programs for counting viral
66 plaques for each well plate (Smith et al., 2013; Sukupolvi-Petty et al., 2013). However, the
67 program has limitations: it cannot be easily optimized and standardized for various viral plaques.
68 Moreover, commercial machines and their services are often expensive and proprietary.
69   For plaque counting on a personal computer, general image-processing tools, such as ImageJ,
70 OpenCV, Labview, R, have been employed (Boonyasuppayakorn et al., 2016; Rasband, 2015; R
71 Core Team, 2016; Cai Z et al., 2011, Cacciabue, Currá, & Gismondi, 2019; Geissmann, 2013,
72 Katzelnick et al., 2018; Moorman & Dong, 2012). Boonyasuppayakorn et al. (2016) developed
73 an ImageJ program and employed it for a modified 96-well plaque assay for the dengue virus. A
74 flatbed scanner was used in the assay to acquire the 96-well plate image before cropping it into
75 each well image. However, the plate must be contrast-enhanced by adding nontransparent liquid,
76 such as milk, before scanning, which increases the workload. Work in several studies (Cai Z et
77 al., 2011, Cacciabue, Currá, & Gismondi, 2019; Geissmann, 2013, Katzelnick et al., 2018;
78 Moorman & Dong, 2012) have developed programs to count viral plaque based on image
79 segmentation, morphological analysis, and image threshold, but the programs require image-
80 processing knowledge to implement and may not be suitable for some assays. To date, no
81 machine learning (ML)-based program has been developed for plaque counting.
82   Due to the need of reducing the number of staff that conduct viral plaque assay, we
83 developed an automated quantification machine based on ML. The machine comprises the
84 hardware system for image acquisition and ML-based software for image viral plaque counting.
85 The hardware is relatively simple to set up, affordable, portable, and automatically acquires a
86 single image or multiple images from a multiwell plate for users. The software is implemented
87 using K-mean clustering, which is a ML algorithm and unsupervised learning algorithm to help
88 users. The algorithm helps by reducing the number of setup parameters for counting.
89   The automated quantification machine was built and evaluated with 96-well plates of dengue
90 virus. The processes for standardizing the manual and software counting algorithm and
91 evaluating the performance of the system on several plaque images are described in the next
92 section. The counting results from the machine are consistent with those from manual counting.
93

Materials & Methods

94

A. Cell and Viruses

95
96 Simplified dengue microwell plaque assays were performed following the procedure reported in
97 Boonyasuppayakorn et al. (2016). In summary, the10-fold serially diluted viruses in a
98 maintenance medium to 10^{-6} were used as the reference. LLC/MK2 (ATCC®CCL-7) cells at 1 x
99 10^4 cells per well (50 μl) of a 96-well plate were mixed with all dilutions and undiluted samples.
100 Then, the dilution was prepared and the cells were incubated as explained in Boonyasuppayakorn
101 et al. (2016). Finally, the dengue virus cells were fixed and then stained as the standard assay.
102 The number of plaque-forming units (p.f.u.) per ml was determined manually and using the
103 automated quantification machine for evaluation.
104

B. Automated Quantification Machine

The automated quantification machine was developed to acquire viral plaque images of each well plate and automatically display the counting results in an easy-to-use manner. The major components of the machine are the hardware for image acquisition and ML-based software for image viral plaque counting.

1) Hardware for Image Acquisition

The automated quantification machine was developed to reduce workload and enable personal use in laboratories. Thus, the machine is relatively simple to set up, affordable, portable, and automatically acquires single or multiple images from multiwell plates for users. Then, the hardware components of the machine include an IAI Tabletop, Model TT-A3-I-2020-10B-SP (IAI Robot, 2021), a USB microscope camera, Dino-Lite AM4113T (AnMo Electronics Corporation, 2021), and an adjustable light source panel, 150 mm × 150 mm surface LED illumination source.

Figure 1: Automated quantification machine.
(A) Prototype of automated quantification machine. (B) Schematic of automated quantification machine.

A photo and a schematic of the automated quantification machine are shown in Figs. 1A and 1B, respectively. The IAI Tabletop is a 3-axis Cartesian robot with a working space of 200 mm × 200 mm × 100 mm (x-, y-, and z-axis). Its repeating positioning accuracy is less than ±0.02 mm. The x-axis of the IAI Tabletop is installed with the multiwell plate fixture and the light source panel and the z-axis is installed with a camera holder and a USB microscope camera. With the Cartesian robot configuration, the IAI Tabletop can move a multiwell plate along the x–y plane for automatic and accurate positioning to capture the well images with the USB microscope camera and move the USB microscope camera along the z-axis to automatically focus the image.

The USB microscope camera is a color camera with a resolution of 1280 × 1024 pixels and 10×–50×, 220× magnification range. It is equipped with an LED coaxial light source. With low magnification, the camera can capture a full-size well image of a six-well plate, and with medium magnification, the camera can capture a full-size well image of a ninety-six-well plate. To change the magnification of the camera, the magnification ring is manually adjusted.

The adjustable light source panel is a square surface LED illumination source. It is installed on the x-axis of the IAI Tabletop and underneath the multiwell plate fixture. The light source panel has high parallelism of light. The high parallelism of the light source panel renders the object edges clearer and sharper in an image. For viral plaque counting, the back-light technique is employed since it gives better image quality than the bright- and dark-field techniques. The back-light technique can be performed by turning off the LED coaxial light source and turning on the light source panel.

To control the machine hardware, the hardware is connected to a personal computer via USB cables and is controlled by a window application developed using C# language. The window

145 application communicates to the IAI Tabletop by PSEL protocol to control the position of the
146 multiwell plate. It also communicates to the USB microscope camera by DNVIT SDK to control
147 the coaxial light source and image acquisition (AnMo Electronics Corporation, 2021). Images
148 are saved in PNG format. The user interface and user experience (UI/UX) design was considered
149 in creating the window application. The window application consists of 1. calibration routine 2.
150 single image and multiwell plate image acquisition 3. Firebase database (Google, 2021).

151 The calibration routine is used to calibrate the movement of the IAI Tabletop. A screenshot
152 of the calibration control is shown in Fig. 2A. Due to the installation process, the coordinate of
153 the multiwell plate fixture is not the same as the coordinate of the IAI Tabletop. This causes the
154 misalignment of the well center position when capturing an image. To apply the calibration
155 routine, the user can work in two steps. The first step is to control the IAI Tabletop by UI control
156 to locate the A1, A12, and H1 well center positions, as shown in Fig. 2A. The second step is to
157 click the calibration routine button. Then, the algorithm automatically recalculates the new
158 coordinate of the IAI Tabletop and makes the coordinate of the multiwell plate fixture and IAI
159 Tabletop the same.

160 The single and multiwell plate image acquisition allows the user to select how to acquire well
161 images. A screenshot of the image acquisition control is shown in Fig. 2B. With the single image
162 acquisition, the user only selects or keys in the desired well number, such as A1, B2, and H12.
163 Then, the machine moves, captures, and displays the desired well image. Moreover, with the
164 multiwell plate image acquisition, the user only clicks one button to make the machine
165 automatically capture and display all multiwell plates. For the 96-well plate, the machine can
166 capture and display all images within less than 1 min. Once images are captured, the user may
167 use the ML-based software for image viral plaque counting.

168 The Firebase database is used to collect all results of the machine for backup. The data in the
169 Firebase database allows new features of the machine to be developed in the future, such as the
170 data storage and exploration features, data analysis tools, data dashboard, web applications, and
171 remote operation. These will provide greater convenience to users.

172

173 Figure 2: Screenshot of calibration control and image acquisition control.
174 (A) Calibration control. (B) Image acquisition control.

175

176 **2) Machine Learning Software for Image Viral Plaque Counting**
177 The algorithm for image viral plaque counting is ML and K-mean clustering (Arora & Varshney,
178 2016). It helps users and reduces the number of setup parameters for counting. The algorithm is
179 also implemented in a window application developed by visual studio C# language and image-
180 processing library, MVtec Halcon (MVTec Software GmbH, 2021a).
181 The viral plaque is surrounded by noninfected cells and is identified using a counterstain,
182 typically a neutral red or crystal violet solution. The white areas indicate the virus plaques, which
183 cause the solution around them to degrade. To count the viral plaques, three major steps are

184 taken to process each image: locating the well position, filtering the color image for image
185 enhancement, and counting the number of viral plaques with K-mean clustering.
186   The region of interest (ROI) is the focus region, which is important for counting viral
187 plaques. The ROI is determined first, followed by the algorithms applied to the corrected
188 location to prevent algorithm error. To locate the well position, a shape-based matching
189 algorithm is employed to find the best matches of a shape model in an image (MVTec Software
190 GmbH, 2021b). It does not use the gray values of pixels and their neighborhood as a template,
191 but it defines the model by the shape of contours. In this case, the circular shape of the well is
192 used as the template. Then, the algorithm finds the best-matched instance of the shape model.
193 The position and rotation of the found instances of the model are returned in the pixel
194 coordinates and angle, which are used to create the ROI image.
195   There are many techniques for filtering color images for image enhancement, including
196 converting the RGB color space to HSV color space or binary image and applying a mean filter.
197 Herein, the CIELAB color space is employed (MVTec Software GmbH, 2021a; Ly, 2020). It
198 presents a quantitative relationship of color on three axes: L* represents the lightness, a*
199 represents the red–green component of a color, and b* represents the yellow–blue component of
200 a color. The CIELAB color space decouples the relationship between lightness and color of an
201 image. Thus, the image brightness is less effective for image-processing. Only a* and b* are
202 used to convert the image to a binary image. The a* and b* values of image pixels in ROI are
203 used for clustering into the two groups, white and dark groups, by K-mean clustering, as shown
204 in Fig. 3A. The yellow area represents the white group or white area, and the blue area represents
205 the dark group or dark area. The red dot represents the centroid of each area. The result of the
206 binary image is shown in Fig. 3B. After this process, a mean filtering process is applied to the
207 binary image.
208
209 Figure 3: Converting RGB image to binary image.
210 (A) a* and b* values of image pixels. (B) Binary image by K-mean clustering
211
212   To count the number of viral plaques, a simple image threshold is employed for region
213 selection. The suspected viral plaque regions are selected and analyzed. An example of suspect
214 regions is shown in Fig. 4A. If the size, length, area, and roundness of a region are appropriated,
215 the region is counted as the viral plaques. An example is shown in Fig. 4B. However, if the size
216 and area of a region are too large because of their overlay, the K-mean clustering is employed in
217 the region. To do that, the grid points are generated inside the large regions along the x–y
218 coordinate, as shown in Fig. 4C. Then, K-mean clustering is employed to cluster the grid points.
219 Moreover, to determine the optimal value of k or the appropriate cluster number, the Silhouette
220 algorithm (Ogbuabor & Ugwoke, 2018) is implemented. The grid points are clustered into k
221 clusters by K-mean clustering. Then, the average Silhouette coefficients for each k cluster are
222 calculated. The Silhouette plot is shown in Fig. 4D. The maximum value of the average
223 Silhouette coefficients is considered the optimal number of clusters. Finally, the number of viral

224 plaques is the summation of the optimal number of clusters and the previous number of viral
225 plaques (Fig. 4E).
226
227 Figure 4: Viral plaque counting with K-mean clustering algorithm.
228 (A) Suspect viral plaque regions. (B) Appropriated region. (C) Grid points inside the larger
229 region. (D) Silhouette plot. (E) Final result.
230
231   A flowchart of the ML-based software for image viral plaque counting is shown in Fig. 5,
232 and an example of the machine counting results is shown in Fig. 6.
233
234 Figure 5: Machine learning (ML)-based software for image viral plaque counting.
235
236 Figure 6: Example of machine counting.
237 (A) Counting results by an expert. (B) Counting by machine.
238
Viral Plaque Reading Differences by Humans
240 Plaque assays were created at the Medical Virology Research Center, Chulalongkorn University,
241 Thailand. More than 25 96-well plates of dengue virus were used to evaluate differences in viral
242 plaque readings. The number of viral plaques from 96-well plates was read by six experts, which
243 included 1,777 wells that could be read by all experts. The remaining wells could not be read by
244 experts, either because they were unclear or because no viral plaques were present; hence, they
245 were not included in the evaluation. The number of viral plaques read by experts ranged between
246 0 and 31. To evaluate variations in expert readings, a boxplot of expert reading results for a
247 given number of viral plaques is presented in Fig. 7. Since the actual number of viral plaques is
248 unknown, the mode value of six expert readings was used as a reference in this case. Data that
249 had no mode was not included in the evaluation. Figure 7(A) shows the distribution of readings
250 by all experts for each number of viral plaques and Figure 7(B) shows an example reading
251 distribution by an expert for different numbers of viral plaques.
252
253 Figure 7: Expert reading distributions.
254 (A) Reading distribution of all experts for each number of viral plaques. (B) Reading distribution
255 examples of an expert for each number of viral plaques. The red + marks represent the outliners
256 of the measurement. The blue line having the slope of 1 represents the measurement reference
257 values. The red dashed line represents the trend line of the measurement results of experts.
258
259   Figure 7 shows that the expert reading distributions in the range of 0–3 are small, but the
260 distribution of expert readings increases when the number of viral plaques increased. When the
261 number of viral plaques exceeds 12, the range of possible readings by an expert varies by more
262 than a factor of 5.

263   To understand the variation in expert readings, a gage repeatability and reproducibility
264   (R&R) analysis was employed (Automotive Industry Action Group, 2010; Burdick, Borror &
265   Montgomer, 2005). A random sample of 300 wells (part) with and without viral plaques was
266   used, in which the number of viral plaques varied from 0–25. Each well was subsequently read
267   by six experts/operators. The results of the gage R&R were evaluated using a nested model (The
268   MathWorks Inc., 2021) and analysis of the expert data was executed in MATLAB (The
269   MathWorks Inc., 2021) using the MATLAB Toolbox to examine the results.
270   The gage R&R analysis was performed for various numbers of viral plaques in six ranges: 0–
271   1, 2–3, 4–8, 9–10, 11–15, 16-25, and 0–25. The results are shown in Table 1.
272   Table 1 indicates that in the range of 0–1, the variation or sigma of expert readings according
273   to the R&R process is 0.9406. The variation or sigma increases as the range of viral plaque
274   numbers increases. The variation or sigma reaches as high as 4.6900 in the range of 16–25. For
275   the overall range of 0–25, the variation or sigma is 2.8063. The reading distribution and reading
276   variation values were used to design the experiment setup described in the following section.
277
278   TABLE 1. Gage repeatability and reproducibility (R&R) analysis for each range of viral plaque
279   numbers.
280

Experiment

282   More than 25 96-well plates of dengue virus were used to evaluate the automated quantification
283   machine. The 96-well plates were put in the machine, and their images were captured. Then, the
284   images were screened for evaluation. There were 1,777 images qualified for evaluation. Next,
285   the number of viral plaques in each image was manually determined by six experts from the
286   research center and by the automated quantification machine software (note that 721 images
287   showed 0 viral plaque). The number of viral plaques was evaluated based on the mode of expert
288   readings and well as by the machine.
289   In the case of many viral plaques in an image, the image was ambiguous. For this reason, the
290   number of viral plaques complicated efforts by the experts to read them. Therefore, an
291   experimental counting criteria was defined based on the reading distribution in Fig. 7, the
292   variation in expert readings in Table 1, and the criterion of the Medical Virology Research
293   Center. If the difference between the number of viral plaques counted by the expert reading
294   mode and the machine is within the maximum number of errors (Table 2), the number of viral
295   plaques counted by the machine is correct. This counting criterion was employed in the
296   evaluation, and the results are presented in the Results section.
297
298   TABLE 2. Maximum number of errors for the software evaluation
299
300   The gage R&R analysis was employed to evaluate the repeatability and reproducibility of the
301   machine (Automotive Industry Action Group, 2010; Burdick, Borror & Montgomer, 2005). For
302   the analysis, 240 wells (part) with and without viral plaques were used. Due to the number of

303 samples, the number of viral plaques of the 240 wells varied from 0 to 18. Then, each well was
304 put into the machine to be captured the image and count the number of viral plaques. This
305 procedure was repeated three times to represent three operators using the machine to count the
306 number of viral plaques. Finally, each well has three measurement results from the machine. The
307 gage R&R using the nested model is employed to evaluate the results (The MathWorks Inc.,
308 2021).
309   MATLAB and MATLAB Toolbox were used to perform the analysis and the gage R&R
310 analysis of the machine data.
311
312 **Results**
313 **A. Distribution Software Counting for Each Number of Viral Plaques**
314 The measurement of the number of viral plaques is depicted in Fig. 8. There are 1,777
315 measurements in the range of 0 to 29 viral plaques. For each number of viral plaques, the boxplot
316 is used to show the mean and distribution of the measurement by the machine. The red + marks
317 represent the outliners of the measurement, which includes less than 5% of the measurement.
318 The boxplot shows that in the range of 0 to 9 viral plaques, the standard deviation (SD) of the
319 measurement is less than 1, and the SD increases as the number of viral plaques increases.
320   The blue line having the slope of 1 represents the measurement reference values. The red
321 dashed line represents the trend line of the measurement results of the machine. The number of
322 viral plaques obtained by the machine ranges from 0 to 29, as calculated form From Fig. 8A
323 using Eq. (1). The goodness-of-fit equation generated an R^2 of 0.8408.

$$y = 0.8054 \times x, \tag{1a}$$

325 Goodness-of-fit:

$$R^2 = 0.8408, \tag{1b}$$

327 where y is the number of viral plaques by the machine, and x is the number of viral plaques by
328 the expert. The values range from 0 to 29.
329   For Fig. 8B, the trendline of the measurement results of the machine shows the number of
330 viral plagues ranging from 0 to 12, as calculated using Eq. (2). The goodness-of-fit equation
331 generated an R^2 of 0.8870.

$$y = 0.9539 \times x, \tag{2a}$$

333 Goodness-of-fit:

$$R^2 = 0.8870. \tag{2b}$$

335   In the range of 0 to 29 viral plaques, the slope of the trend line of the machine is 0.8054,
336 whereas, in the range of 0 to 12 viral plaques, the slope is 0.9539. For a number of viral plaques
337 in the range of 0–12, the line has a slope close to 1 with R^2 of 0.8870. Therefore, the counting
338 results by the machine and experts correspond to the highest evaluation quality. Moreover, to
339 evaluate the correlation between the counting by the expert and machine, Pearson's coefficient
340 method was used to measure the strength of the association between the machine and manual
341 counting (Mukaka, 2021). The Pearson's coefficient r of these variables is 0.9221 with a p-value
342 of less than 0.0001. Since the p-value is less than 0.05, the variables reliably correlate.
343

344   Figure 8: Distribution software counting for each number of viral plaques.
345   (A) Distribution of software counting for each number of viral plaques. (B) Distribution of
346   software counting for the range [0–12] of number of viral plaques. The red + marks represent the
347   outliners of the measurement. The blue line having the slope of 1 represents the measurement
348   reference values. The red dashed line represents the trend line of the measurement results of the
349   machine.
350

351   **B. Bland–Altman**
352   To evaluate the performance of the machine, the Bland–Altman plot was used (Myles, 2007).
353   The measurements from the expert and machine were considered. The difference in the
354   measurement results from the expert and machine, error mean bias, and error SD were
355   determined. The Bland–Altman plot is shown in Fig. 9. The results indicate that 95.01% of the
356   measurement error is in the upper and lower boundaries (±2 SD). Therefore, the error from the
357   machine is within the boundary limit. The machine effectively and efficiently quantified the
358   number of viral plaques.
359

360   Figure: 9 Bland–Altman plot of the machine measurement results.
361

362   **C. Performance of the Machine**
363   Counting viral plaques is ambiguous, even by an expert. Thus, counting criteria were defined, as
364   shown in Table 2. If the error between the number of viral plaques counted by the expert reading
365   mode and machine is within the maximum number of errors, as shown in Table 2, the number of
366   viral plaques counted by the machine is correct.
367   The counting error between expert mode and the machine is presented using the boxplot (Fig.
368   10). The magenta line presents the maximum number of errors for each reference number of viral
369   plaques. Figure 10 shows that in the range of 0–18 viral plaques, the mean measurements of the
370   machine are within the boundary error, and the error is acceptable. For the range of 19–29 viral
371   plaques, the error is large and out of the boundary. Consequently, when the number of viral
372   plaques is larger, it is more difficult to measure the number of viral plaques. The accuracy of the
373   reading from the large number is not significant to quantify viral infection or research. Moreover,
374   only 55 of the 1,777 images are in the range of 19–29 viral plaques.
375

376   Figure 10: Distribution software error for each number of viral plaques.
377

378   Based on the criteria in Table 2, the percentage of correct and incorrect measurements by the
379   machine is shown in Fig. 11. The light blue bar represents the percentage of correct measurement
380   which the machine measurement and expert reading mode are exactly the same. The dark blue
381   bar represents the percentage of correct measurement which the machine measurement is within
382   the defined range of expert reading mode and the red bar represents the percentage of incorrect
383   measurement of the machine. The percentage of correct measurement is high when the number

384   of viral plaques is low. In the range of 0–29 viral plaques, the percentage of correct measurement
385   is more than 80%. In addition, the average correct measurement by the machine is 85.8%. This
386   number is consisted of the percentages of exact correct and within the range are 60.0% and
387   25.8%, respectively.
388
389   Figure 11: Percentage of correct measurement by the machine.
390
391   **D. R&R of the Machine**
392   The R&R of the machine was evaluated by gage R&R analysis according to Automotive
393   Industry Action Group (2010) and Burdick, Borror & Montgomer (2005). The gage R&R is
394   shown in Table 3. Previous authors (Automotive Industry Action Group, 2010; Burdick, Borror
395   & Montgomer, 2005) suggest that the measurement system is acceptable if the number of distinct
396   categories (NDC) is greater than or equal to 5. Moreover, for the percentage of gage R&R of
397   total variations (PRR), the measurement system is capable if PRR is less than 10% and not
398   capable if PRR is more than 30%. Otherwise, the measurement system is acceptable.
399   NDC of the machine is 6 and the PRR is 21.72%, which is between 10% and 30% criteria
400   (Table 3). Due to the cost of the machine and previous results and evaluations, the R&R of the
401   machine is acceptable, and the machine is capable of application.
402
403   TABLE 3. Gage R&R analysis parameters for the machine.
404

Discussion

406   Counting the number of viral plaques is ambiguous, even for experts. Consequently, the Medical
407   Virology Research Center defined experimental counting criteria for evaluating the machine
408   output (Table 2) based on the distribution and variation of expert readings. If the number of viral
409   plaques is small, the maximum number of errors is small, and as the number of viral plaques
410   increases, the maximum number of errors increases. However, in the case of a large number of
411   viral plaques, the reading accuracy is not sufficient for quantifying viral infection or in viral
412   research.
413   The automated quantification machine was evaluated using 96-well plates of dengue virus.
414   According to the analysis, the measurement results obtained using the machine correlate well
415   with the manual counting results. For 0–29 viral plaques, the trend line of the result of the
416   machine has a slope of 0.8054 with R^2 of 0.8408, and in the range of 0–12 viral plaques, the
417   slope is 0.9539 with R^2 of 0.8870. The correlation in the range of 0–12 viral plaques is better
418   than that in the range of 0–29 viral plaques.
419   The Pearson's coefficient r of the data is 0.9221 with a p-value of less than 0.0001. This
420   shows that the machine counting results correlate with the manual counting results. Further, the
421   Bland–Altman plot shows that more than 95% of the measurement errors are in the upper and
422   lower boundaries (±2 SD). Thus, the manual and machine counting results are consistent.

423   As shown in Fig. 8B, for 0–12 viral plaques, the boxplot is close to the reference line,
424   indicating the manual and machine counting results are in good agreement. However, for 13–29
425   viral plaques, the boxplot mean is below the reference line, indicating that the measurement
426   results of the machine are less than the manual measurement results. This information can be
427   used to improve the algorithm for measurement in the range of 13–29 viral plaques in future
428   studies.
429   The large error in the results of the machine in the range of 13–29 viral plaques could be
430   attributed to the criteria of the Silhouette algorithm. The Silhouette algorithm uses only the
431   location information of the grid points to calculate the Silhouette score for selecting the suitable
432   number of clusters. To improve the algorithm, other criteria, such as the number of grid points
433   and areas, can be included in the algorithm to calculate the new Silhouette score.
434   Base on the gage R&R analysis, the major variations in PRR results from reproducibility,
435   which occurs when the user puts the sample to the machine and measures the number of viral
436   plaques. If the brightness of the environment light is changed, the image color may be changed,
437   which affects the algorithm. This may be overcome by creating a cover for the machine to reduce
438   the effect of environmental light. The repeatability of the machine is 0 since the counting
439   algorithm has no variation.
440   According to the performance analysis, the average correct measurement of the machine is
441   85.8% in the range of 0–29 viral plaques. However, most of the errors occur when the number of
442   viral plaques is high. If only small and medium numbers of viral plaques are evaluated, the
443   average correct measurement of the machine would be more than 85.8%.
444   The plaque sizes varied by various conditions such as pH of the buffers, concentrations of the
445   semisolid, or under antiviral treatment. Moreover, previous reports have optimized the plaque
446   readings in 24- and 96-well plates in antiviral drug discovery (Boonyasuppayakorn et al., 2016;
447   Katzelnick et al., 2018; Yin et al., 2019). In order to cover this issue, our developed software
448   provides the manually adjustable plaque sizes customized by users. The user can config the
449   parameters the range of plaque sizes, save, and use them for the specific scenario.
450   Even though there are automated imaging-based counters for plaque assay, the current
451   commercial versions have multiple challenges, especially their complexity and cost. They may
452   unsuitable for personal use in the laboratory. Thus, for situations of limited resources, the
453   developed machine may be more suitable for a personal laboratory. Additionally, the developed
454   machine can be applied to Elispot counting (Kukiattikoon et al., 2021).
455

Conclusions

457   The developed automated quantification machine with ML-based software effectively
458   quantified the number of viral plaques in a 96-well plate in a simple process and at a low cost.
459   The automated quantification machine was evaluated using 96-well plates of dengue virus. The
460   performance analysis showed that the machine measurement results correlate well with manual
461   counting results, and the average correct measurement by the machine is 85.8%. The machine

462 meets the requirements of reducing workload and performing virus plaque assay reading in the
463 laboratory.
464

Acknowledgements

466 We thank the Medical Virology Research Center, Chulalongkorn University, Thailand, for
467 helping us with the sample and experiments.
468 Special thanks to CU VISION X for supporting the MVTec Halcon software.

469

References

471 [1] Dulbecco, R., 1952. Production of Plaques in Monolayer Tissue Cultures by Single Particles
472 of an Animal Virus. Proc. Natl. Acad. Sci. U. S. A., 38 (8), 747-752.
473 [2] Premsattham P, Salakij S, Boonyasuppayalorn S, Phanomchoeng G. 2019. Development of
474 Au-welltomated Platform for Image Capturing and Counting Algorithm for Viral Plaque. *ACM*
475 *International Conference Proceeding Series, 3rd International Conference on Virtual and*
476 *Augmented Reality Simulations*. ICVARS 2019. 52-56.
477 [3] BioTek Instruments, Inc. 2021. Automated Viral Plaque Assay Workflow Using the Cytation
478 Cell Imaging Multi-Mode Reader. *Application Bulletin*, Rev. 01/07/21.
479 [4] Cacciabue M, Currá A, Gismondi MI. 2019. ViralPlaque: a Fiji macro for automated
480 assessment of viral plaque statistics. *PeerJ* 7:e7729.
481 [5] Bhattarakosol P, Yoosook C, Cross A. 1990. Intratypic variation of herpessimplex virus type
482 2 isolates detected by monoclonal antibodies against viralglycoproteins. *Arch. Virol*. 115, 89–
483 100.
484 [6] Boonyasuppayakorn S, Suroengrit A, Srivarangkul P, Yuttithamnon W, Pankaew S, Saelee T,
485 Prompetchara E, Salakij S, Bhattarakosol P. 2016. Simplified dengue virus microwell plaque
486 assay using an automatedquantification program. *Journal of Virological Methods*, 237, 25–31.
487 [7] Sullivan K, Kloess J, Qian C, Bell D, Hay A, Lin YP, Gu Y. 2012. High throughput virus
488 plaque quantitation using a flatbed scanner. *Journal of Virological Methods*, 179(1), 81-89.
489 [8] Cellular Technology Limited (CTL). 2021. ImmunoSpot CLT S6 Analyzers, *Available at*
490 *http://www.immunospot.com* (accessed 30 June 2021)
491 [9] Smith SA, deAlwis R, Kose N, Durbin AP, Whitehead SS, deSilva AM, et al. 2013. Human
492 monoclonal antibodies derived from memory B cells following live attenuated dengue virus
493 vaccination or natural infection exhibit similar characteristics. *J Infect Dis*. 207, 1898–1908.
494 [10] Sukupolvi-Petty S, Brien JD, Austin SK, Shrestha B, Swayne S, Kahle K, et al. 2013
495 Functional Analysis of Antibodies against Dengue Virus Type4 Reveals Strain-Dependent
496 Epitope Exposure That Impacts Neutralization and Protection. *J Virol*. 87, 8826–8842.
497 [11] Rasband WS. 1997-2015. *ImageJ. In: National Institutes of Health*, Bethesda, Maryland,
498 USA.
499 [12] R Core Team. 2016. *R: A language and environment for statistical computing*. R
500 Foundation for Statistical Computing. Vienna, Austria.

501 [13] Cai Z Z, Chattopadhyay N, Liu WJ, Chan C, Pignol JP, Reilly RM. 2011. Optimized digital
502 counting colonies of clonogenic assays using ImageJ software and customized macros:
503 comparison with manual counting. *International Journal of Radiation Biology*. 87, 1135-1146.
504 [14] Cacciabue M, Currá A, Gismondi MI. 2019. Viral Plaque: a Fiji macro for automated
505 assessment of viral plaque statistics. *PeerJ*. 7 e7729 http://doi.org/10.7717/peerj.7729.
506 [15] Geissmann Q. 2013. OpenCFU, a new free and open-source software to count cell colonies
507 and other circular objects. *PLOS ONE*. 8(2) e54072 DOI 10.1371/journal.pone.0054072.
508 [16] Katzelnick LC, et. 2018. Viridot: An automated virus plaque (immunofocus) counter for the
509 measurement of serological neutralizing responses with application to dengue virus. *PLoS Negl*
510 *Trop Dis*. 12(10) e0006862.
511 [17] Moorman M, Dong A. 2012. Automated Viral Plaque Counting Using Image Segmentation
512 and Morphological Analysis. *2012 IEEE International Symposium on Multimedia*. 157-160.
513 [18] IAI Robot (Thailand) Co., Ltd. 2021. TT Gantry Type, *Available at https://www.iai-*
514 *robot.co.th/en/product/table/tt.php* (accessed 30 June 2021)
515 [19] AnMo Electronics Corporation. 2021. *Available at https://www.dino-lite.com* (accessed 30
516 June 2021)
517 [20] Google. 2021. Firebase, *Available at https://firebase.google.com* (accessed 30 June 2021)
518 [21] Arora P, Varshney S. 2016. Analysis of k-means and k-medoids algorithm for big data.
519 *Procedia Computer Science*. vol. 78, 507-512.
520 [22] MVTec Software GmbH. 2021. *Solution Guide I Basics Halcon 20.11 Steady*, *Available at*
521 *https://www.mvtec.com* (accessed 30 June 2021)
522 [23] MVTec Software GmbH. 2021 *Solution Guide II-B Matching Halcon 20.11 Steady*,
523 *Available at https://www.mvtec.com* (accessed 30 June 2021)
524 [24] Ly BC, Dyer EB, Feig JL, Chien A, Bino SD. 2020. Research Techniques Made Simple:
525 Cutaneous Colorimetry: A Reliable Technique for Objective Skin Color Measurement. *The*
526 *Journal of investigative dermatology*. 140, 3-12.
527 [25] Ogbuabor G, Ugwoke FN. 2018. Clustering Algorithm for A Healthcare Dataset Using
528 Silhouette Score Value. *Int. J. Comput. Sci. Inf. Technol.*102 (2018) 27–37.
529 [26] Automotive Industry Action Group (AIAG). 2010. *Measurement Systems Analysis*
530 *Reference Manual*, 4th edition. Chrysler, Ford, General Motors Supplier Quality Requirements
531 Task Force.
532 [27] Burdick RK, Borror CM, Montgomer DC. 2005. *Design and Analysis of Gauge R&R*
533 *Studies: Making Decisions with Confidence Intervals in Random and Mixed ANOVA Models*.
534 Society for Industrial Applied Mathematics: American Statistical Association.
535 [28] The MathWorks Inc. Matlab. *Available at https://www.mathworks.com* (accessed 30 June
536 2021)
537 [29] Mukaka MM. 2012. Statistics Corner: A guide to appropriate use of Correlation coefficient
538 in medical research. *Malawi Medical Journal*. 24(3), 69-71.
539 [30] Myles PS, Cui J. 2007. Editorial I Using the Bland–Altman method to measure agreement
540 with repeated measures. *British Journal of Anaesthesia*. 99(3), 309-311.

541   [31] Katzelnick LC, Coello Escoto A, McElvany BD, Chávez C, Salje H, Luo W, et al. 2018.
542   Viridot: An automated virus plaque (immunofocus) counter for the measurement of serological
543   neutralizing responses with application to dengue virus. *PLoS Negl Trop Dis* 12(10): e0006862.
544   https://doi.org/10.1371/journal.pntd.0006862
545   [32] Yin Y, Xu Y, Ou Z, Yang X, Liu H. 2019. An antiviral drug screening system for
546   enterovirus 71 based on an improved plaque assay: A potential high-throughput method. *J Med*
547   *Virol.* 2019 Aug;91(8):1440-1447. doi: 10.1002/jmv.25463. Epub 2019 Apr 1. PMID: 30900754.
548   [33] Kukiattikoon C, Vongsoasup N, Ajavakom N, and Phanomchoeng G. 2021. Automate
549   platform for Capturing and Counting ELISpot on 96-Well Plate. *Proc. of the 7th International*
550   *Conference on Engineering and Emerging Technologies (ICEET)* 27-28 October 2021, Istanbul,
551   Turkey.

TABLE 1. Gage repeatability and reproducibility (R&R) analysis for each range of viral plaque numbers.

TABLE 1. Gage repeatability and reproducibility (R&R) analysis for each range of viral plaque numbers.

	Reference Number of Viral Plaques													
	0-1		2-3		4-8		9-10		11-15		>16		All	
	Var.	Sigma	Var.	Sigma	Var.	Sigma	Var.	Sigma	Var.	Sigma	Var.	Sigma	Var.	Sigma
Gage R&R	0.8847	**0.9406**	1.5433	**1.2423**	6.3720	**2.5243**	7.2413	**2.6910**	9.2160	**3.0358**	21.9960	**4.6900**	7.8756	**2.8063**
Repeatability	0.8510	0.9225	1.2298	1.1090	3.9490	1.9872	5.2781	2.2974	5.3403	2.3109	10.0464	3.1696	5.6792	2.3831
Reproducibility	0.0337	0.1835	0.3136	0.5600	2.4230	1.5566	1.9632	1.4011	3.8757	1.9687	11.9496	3.4568	2.1964	1.4820
Operator	0.0337	0.1835	0.3136	0.5600	2.4230	1.5566	1.9632	1.4011	3.8757	1.9687	11.9496	3.4568	2.1964	1.4820
Part	0.3568	0.5973	0.5092	0.7136	5.4656	2.3379	2.0874	1.4448	4.2479	2.0610	6.3211	2.5142	39.8431	6.3121
Total	1.2415	1.1142	2.0525	1.4327	11.8376	3.4406	9.3288	3.0543	13.4639	3.6693	28.3171	5.3214	47.7187	6.9079

TABLE 2. Maximum number of errors for the software evaluation

1   TABLE 2. Maximum number of errors for the software evaluation

Reference Number of Viral Plaques	Maximum Number of Errors
0-1	± 0
2-3	± 1
4-8	± 2
9-10	± 3
11-15	± 4
>16	± 5

TABLE 3. Gage R&R analysis parameters for the machine.

1   TABLE 3. Gage R&R analysis parameters for the machine.

Source	Variance	%Variance	Sigma	5.15 x sigma	% 5.15 x sigma
Gage R&R	0.8861	4.7196	0.9413	4.8479	21.7246
Repeatability	0.0000	0.0000	0.0000	0.0000	0.0000
Reproducibility	0.8861	4.7196	0.9413	4.8479	21.7246
Operator	0.8861	4.7196	0.9413	4.8479	21.7246
Part	17.8891	95.2804	4.2296	21.7822	97.6117
Total	18.7752	100	4.3330	22.3151	

2   Number of distinct categories (NDC): 6

3   % of Gage R&R of total variations (PRR): 21.72

4   Note: The last column of the above table does not to necessarily sum to 100%

Figure 1

Figure 1: Automated quantification machine.

(A) Prototype of automated quantification machine. (B) Schematic of automated quantification machine.

A

Camera Holder

USB Microscope Camera

Light Source Panel

Multi-Well Plate

Multi-Well Plate Fixture

IAI Tabletop

z-axis

100 mm

200 mm

y-axis

x-axis

200 mm

B

Multi-Well Plate

Results

Mobile Application

USB Cables

Firebase

Automated Quantification Machine
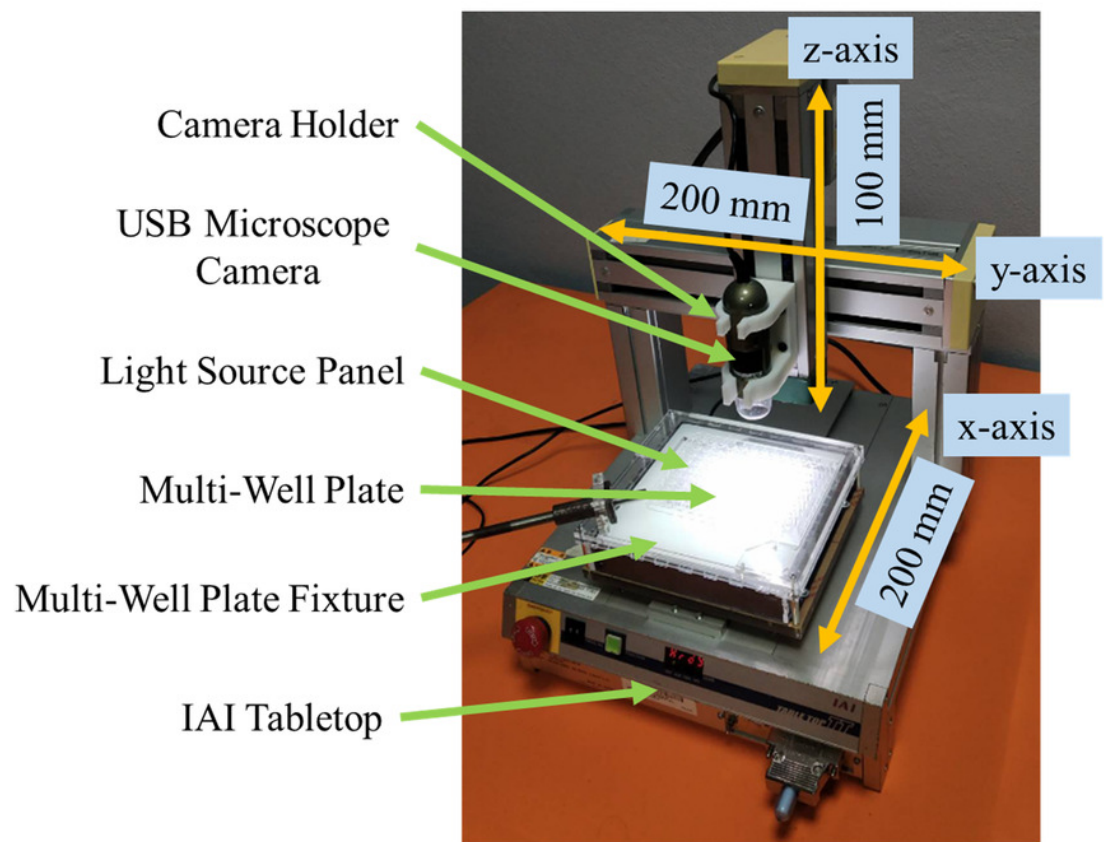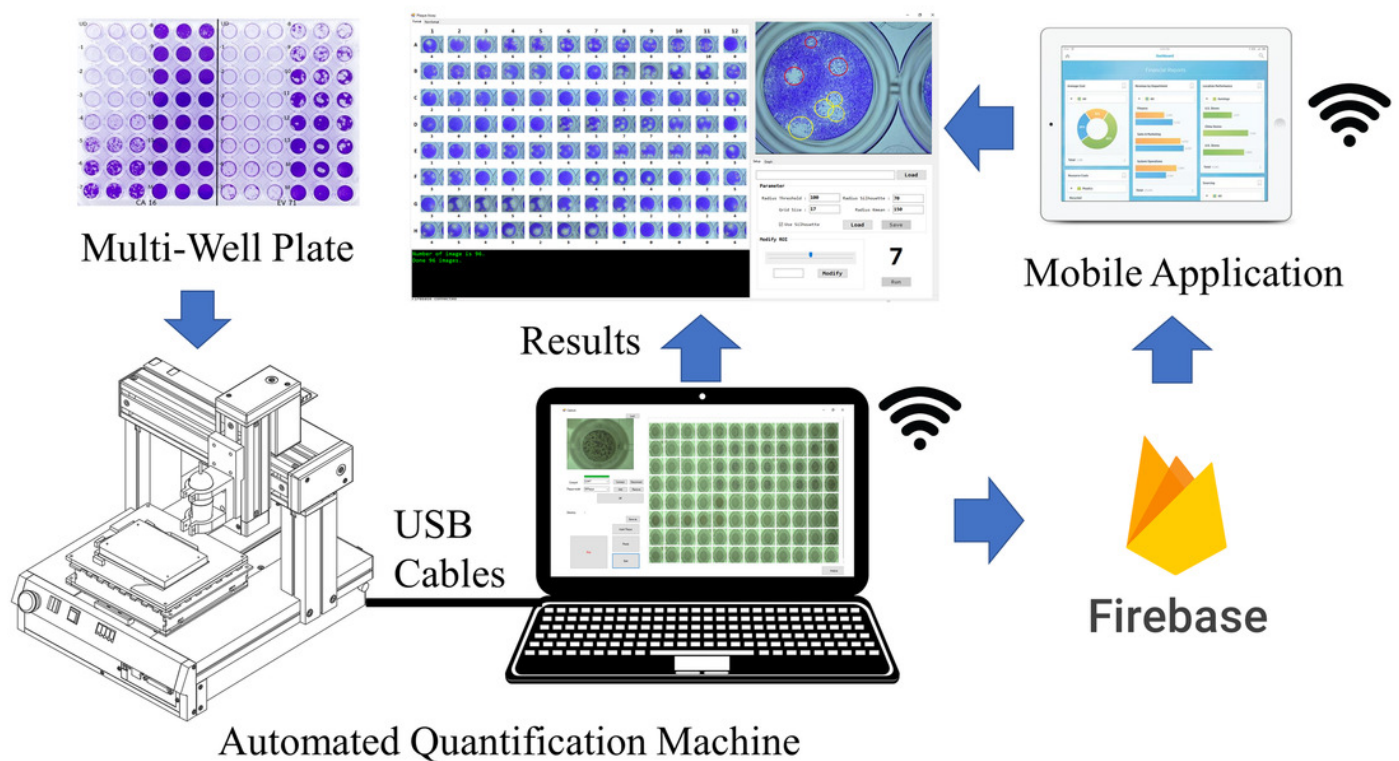
Figure 2

Figure 2: Screenshot of calibration control and image acquisition control.

(A) Calibration control. (B) Image acquisition control.
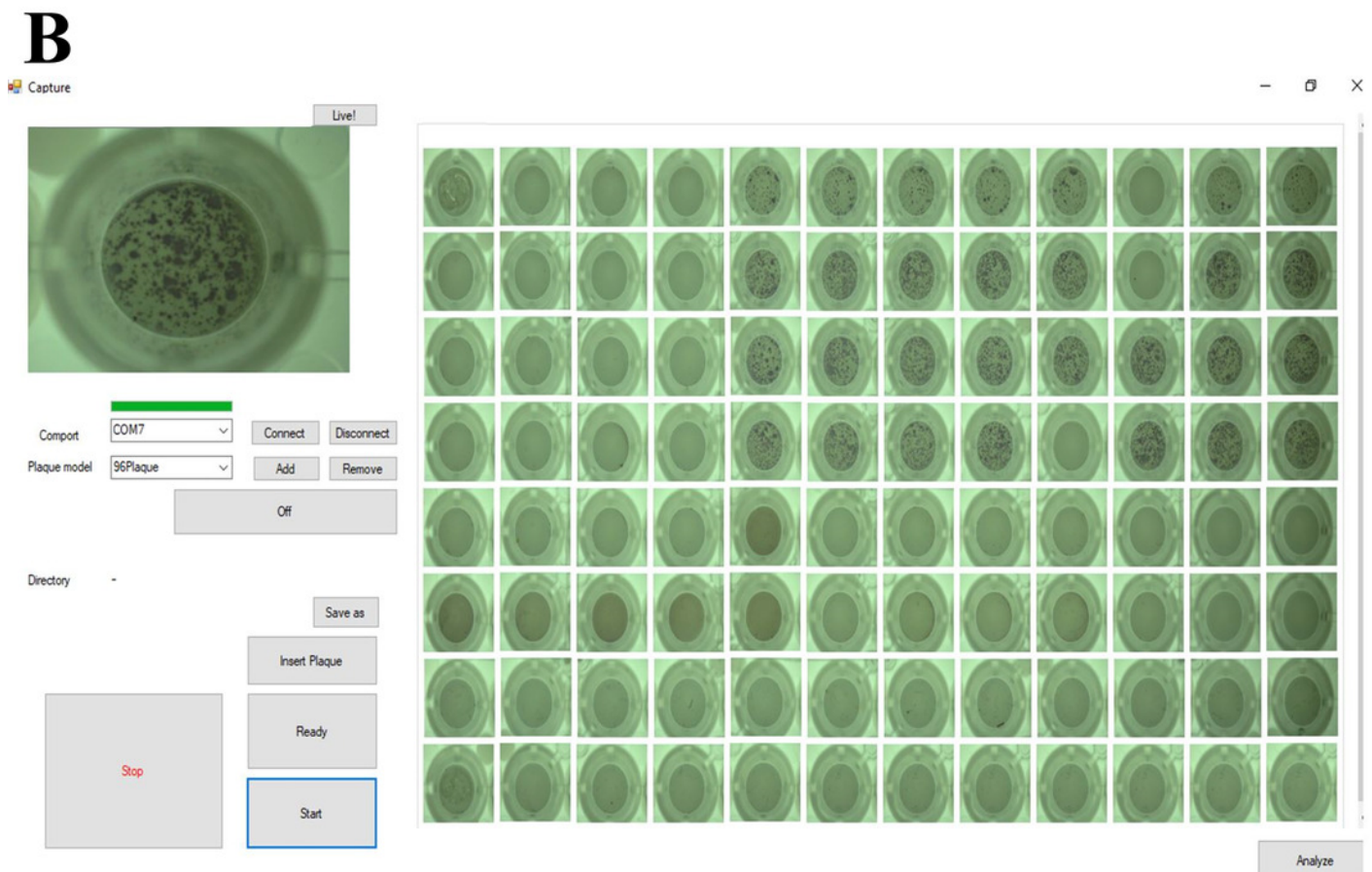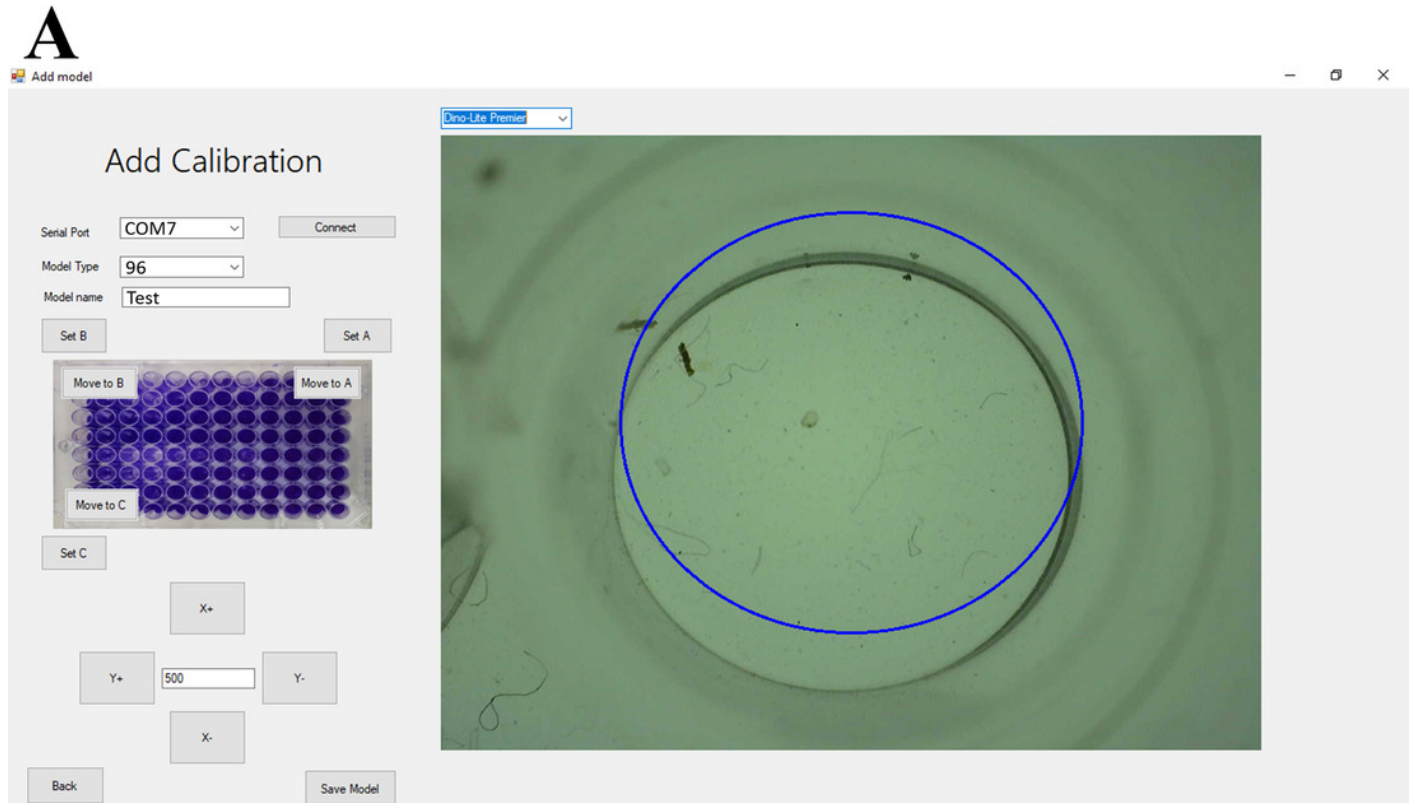
Figure 3

Figure 3: Converting RGB image to binary image.

(A) a* and b* values of image pixels. (B) Binary image by K-mean clustering
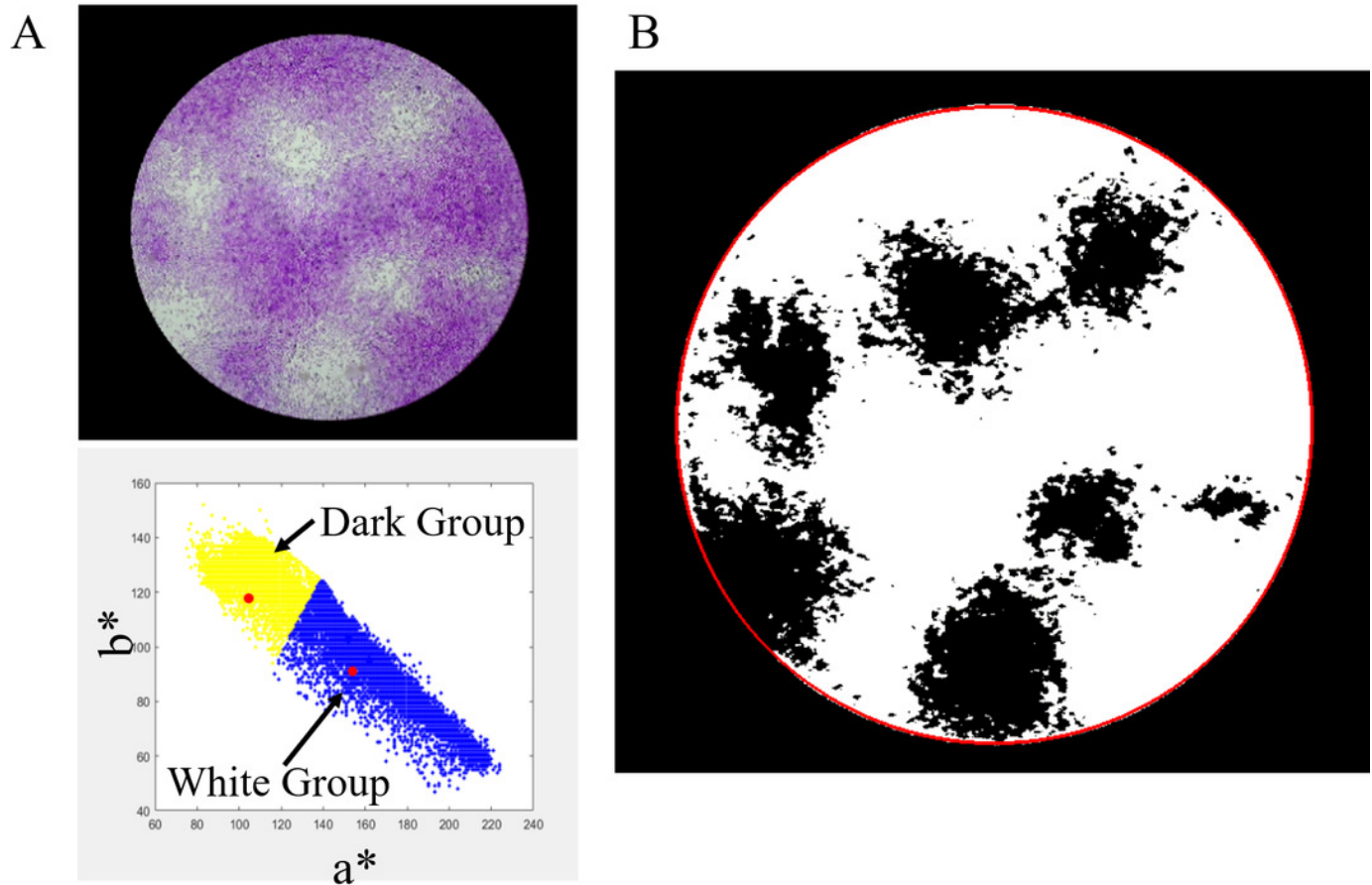
Figure 4

Figure 4: Viral plaque counting with K-mean clustering algorithm.

(A) Suspect viral plaque regions. (B) Appropriated region. (C) Grid points inside the larger region. (D) Silhouette plot. (E) Final result.
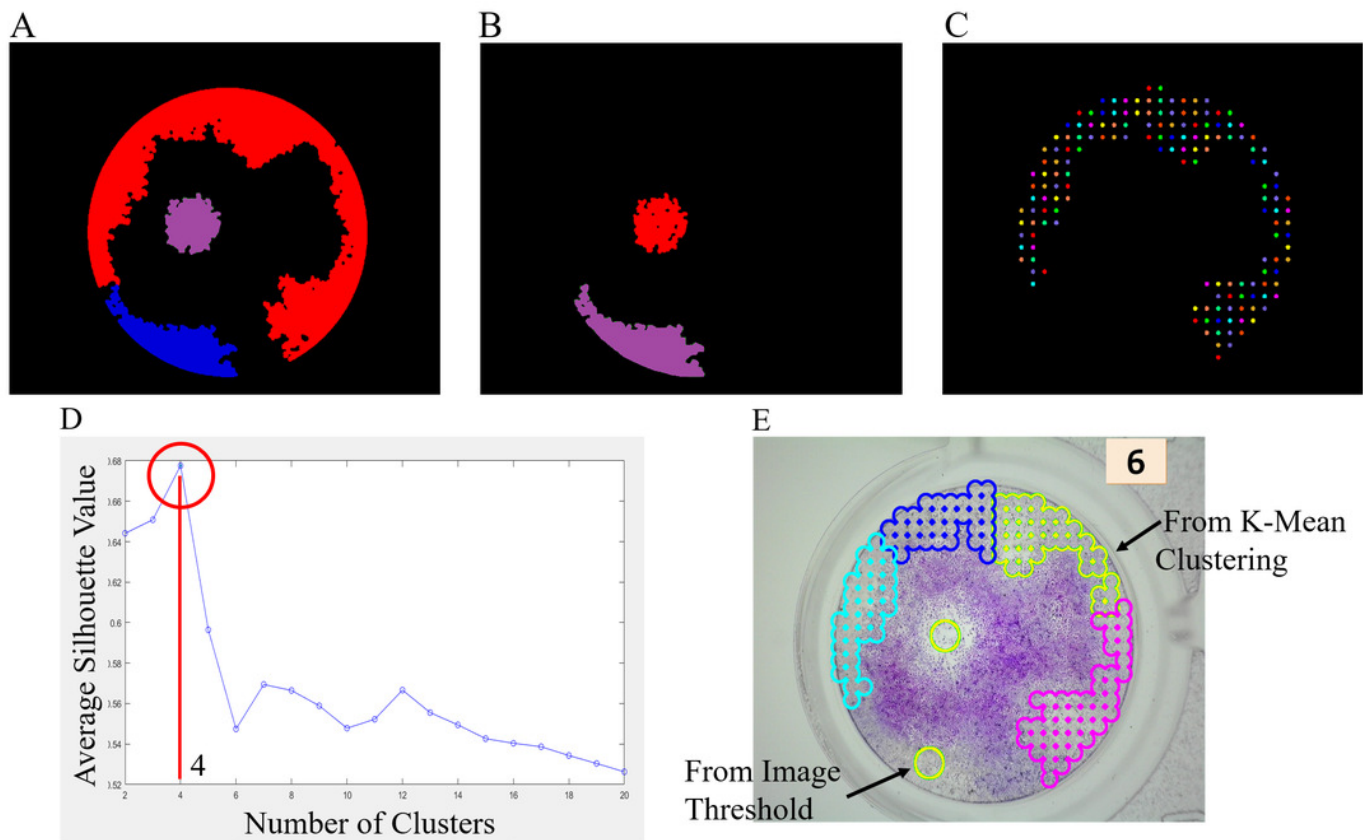
Figure 5

Figure 5: Machine learning (ML)-based software for image viral plaque counting.
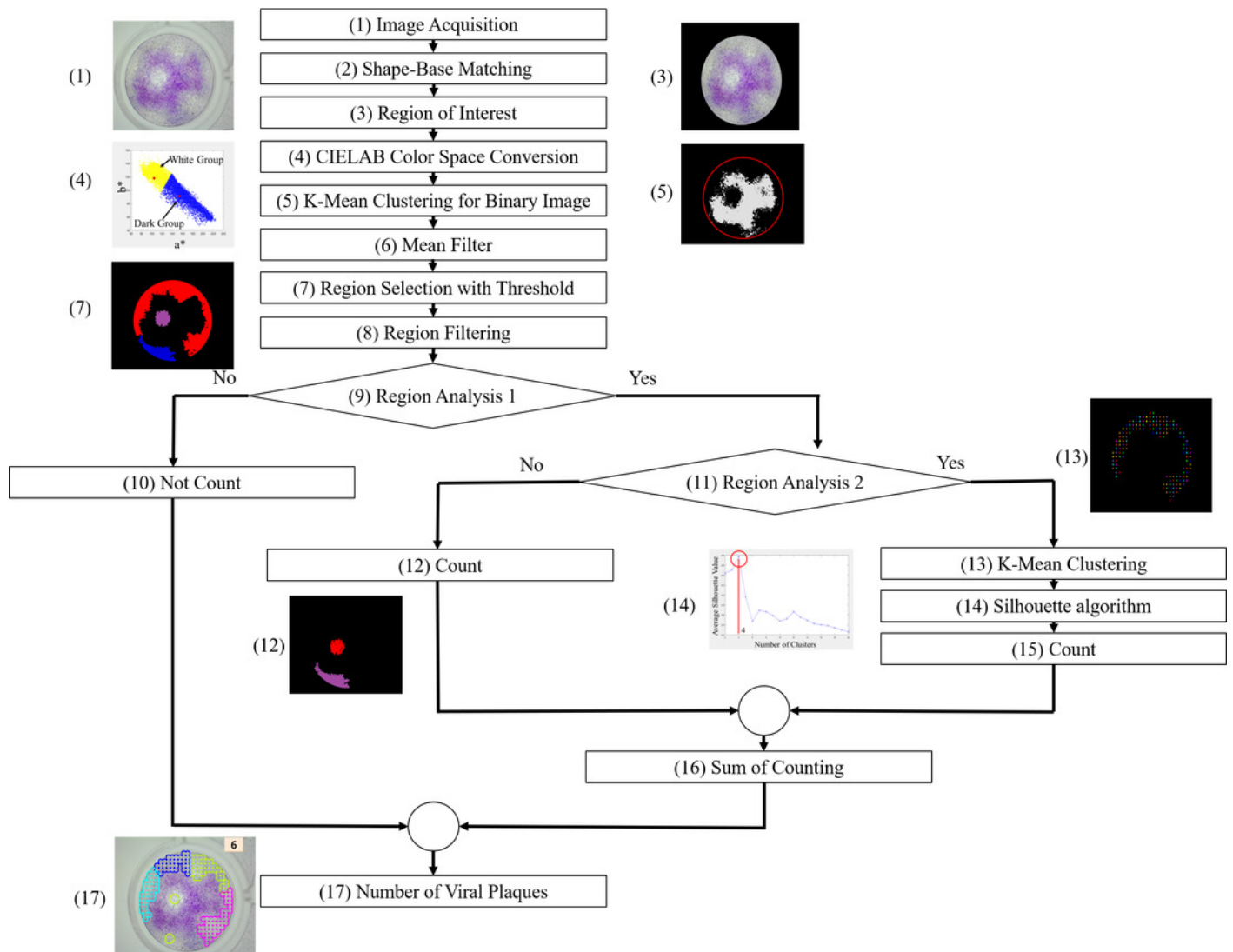
Figure 6

Figure 6: Example of machine counting.

(A) Counting results by an expert. (B) Counting by machine.
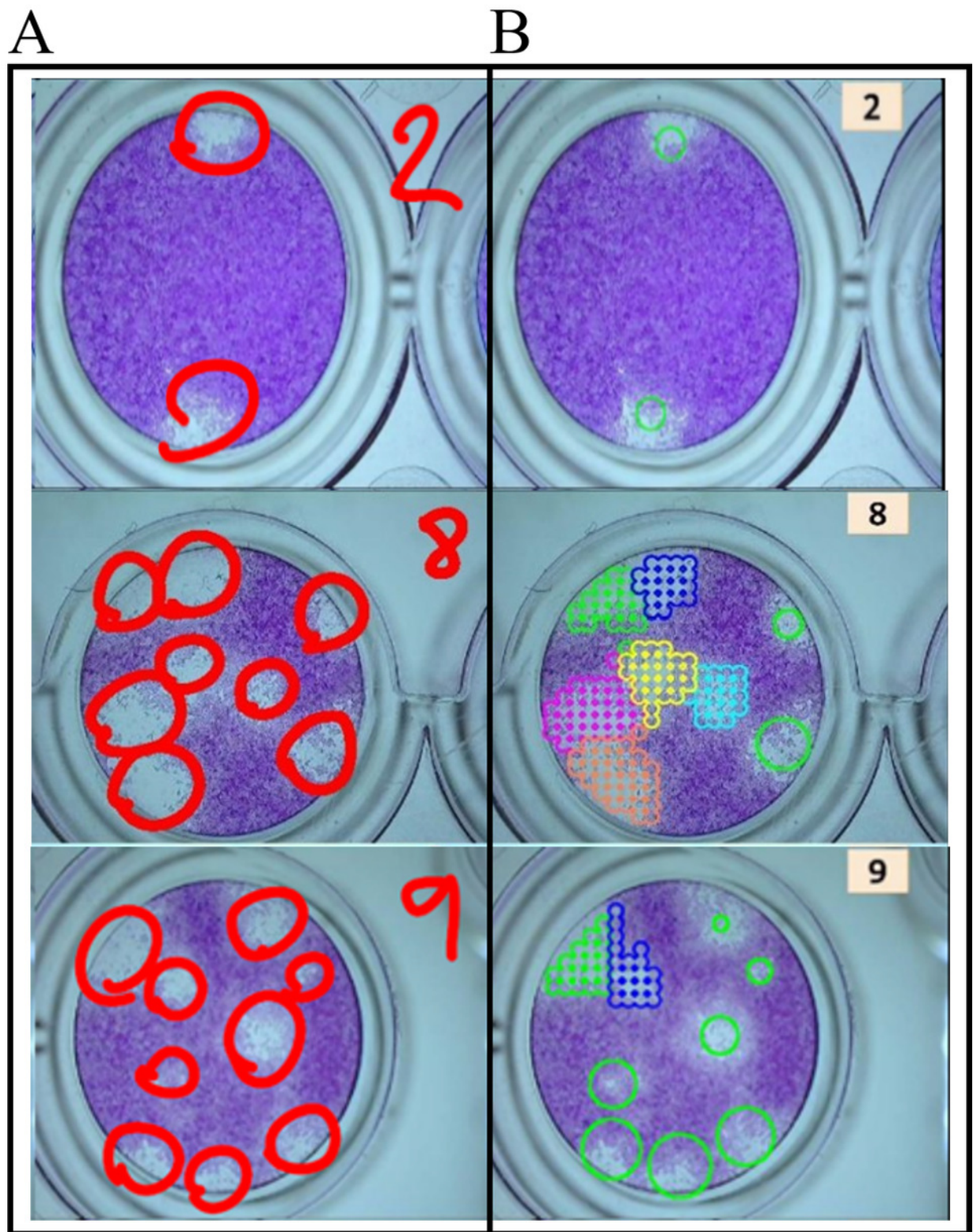
Figure 7

Figure 7: Expert reading distributions.

(A) Reading distribution of all experts for each number of viral plaques. (B) Reading distribution examples of an expert for each number of viral plaques. The red + marks represent the outliners of the measurement. The blue line having the slope of 1 represents the measurement reference values. The red dashed line represents the trend line of the measurement results of experts.
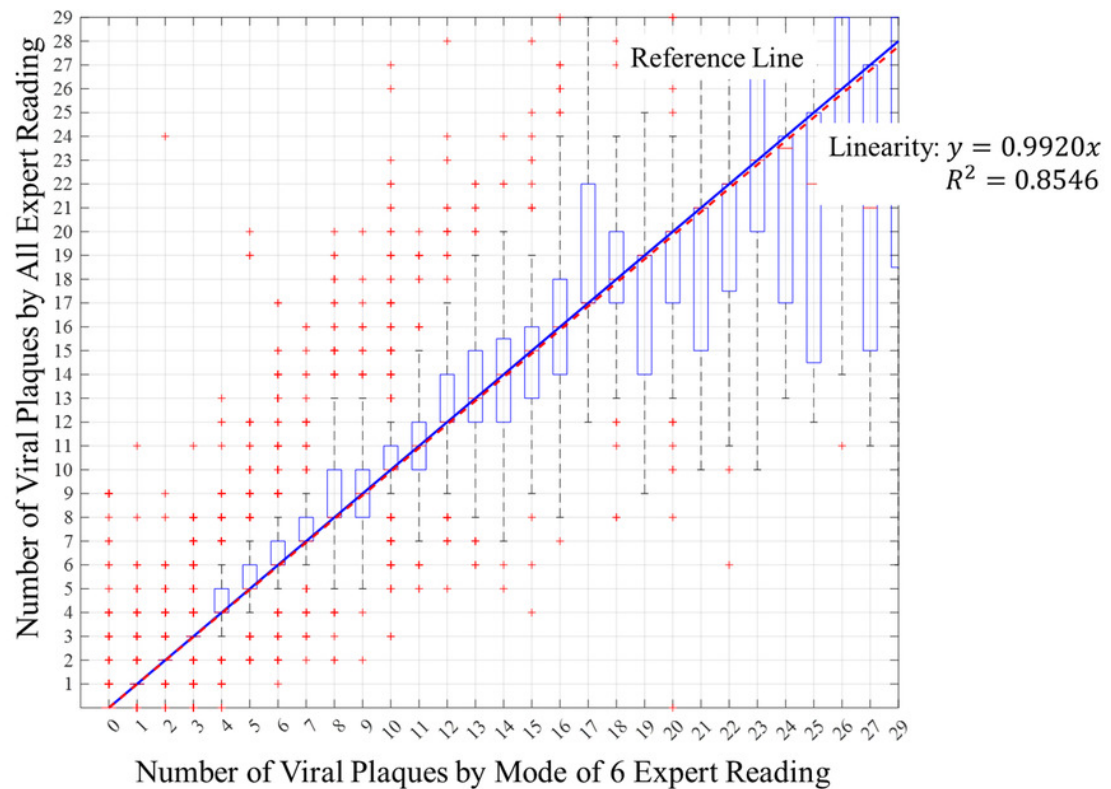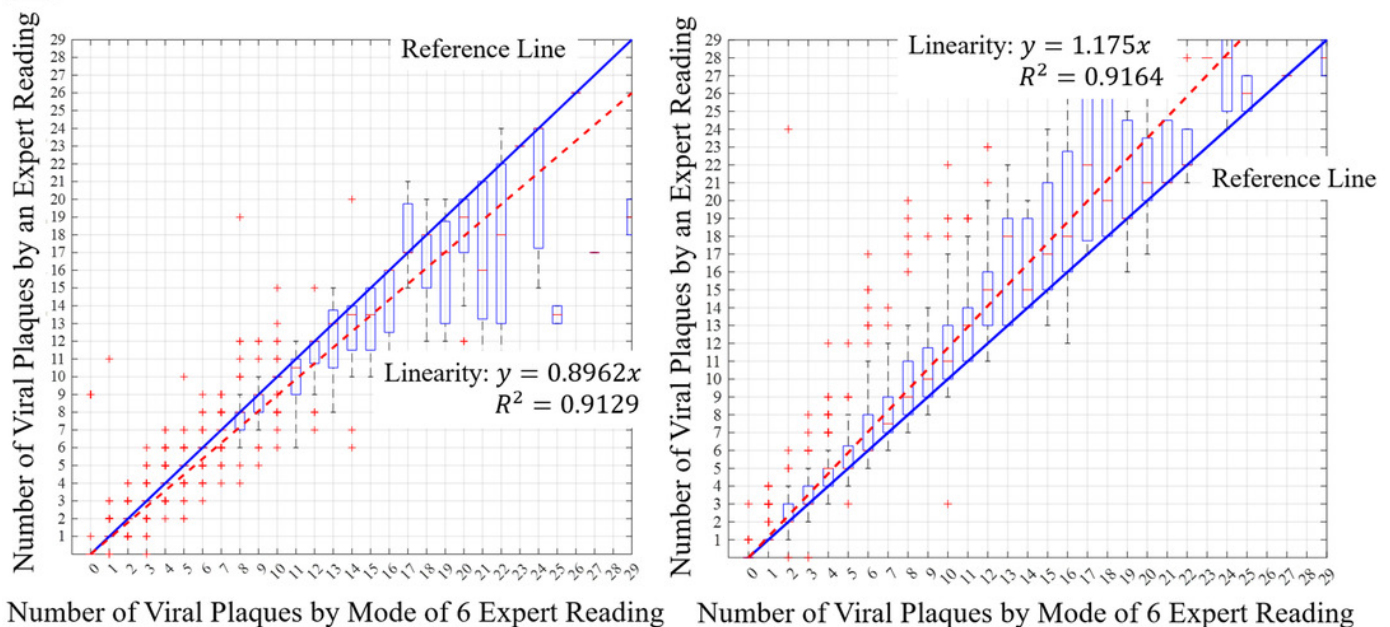
Figure 8

Figure 8: Distribution software counting for each number of viral plaques.

(A) Distribution of software counting for each number of viral plaques. (B) Distribution of software counting for the range [0–12] of number of viral plaques. The red + marks represent the outliners of the measurement. The blue line having the slope of 1 represents the measurement reference values. The red dashed line represents the trend line of the measurement results of the machine.
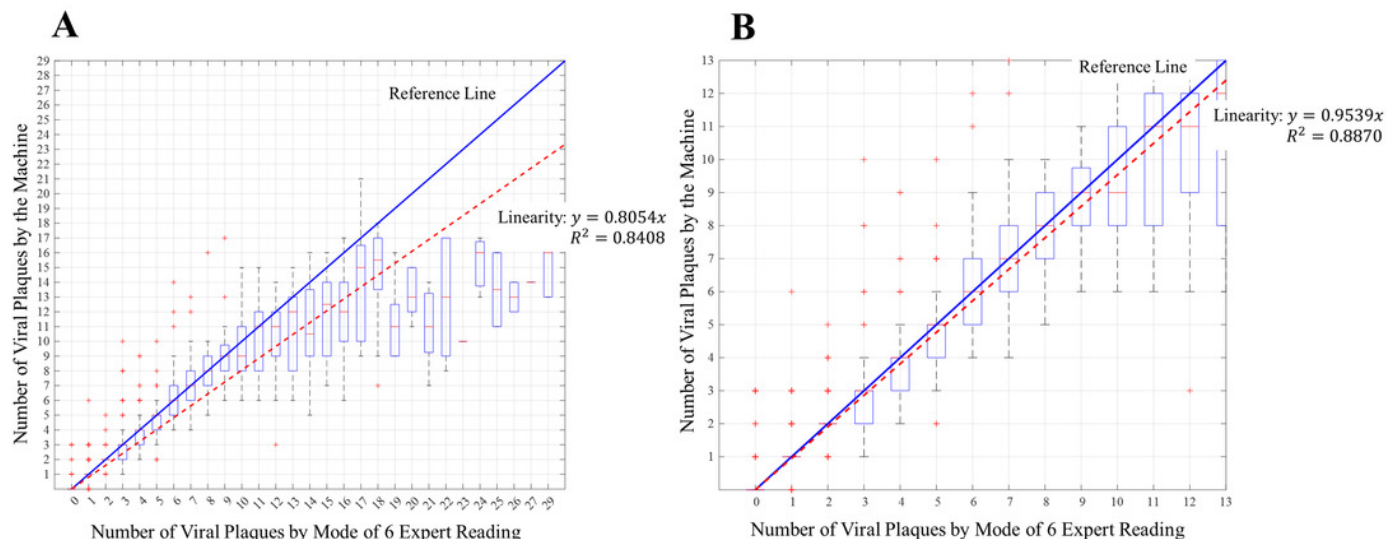
Figure 9

Figure: 9 Bland–Altman plot of the machine measurement results.
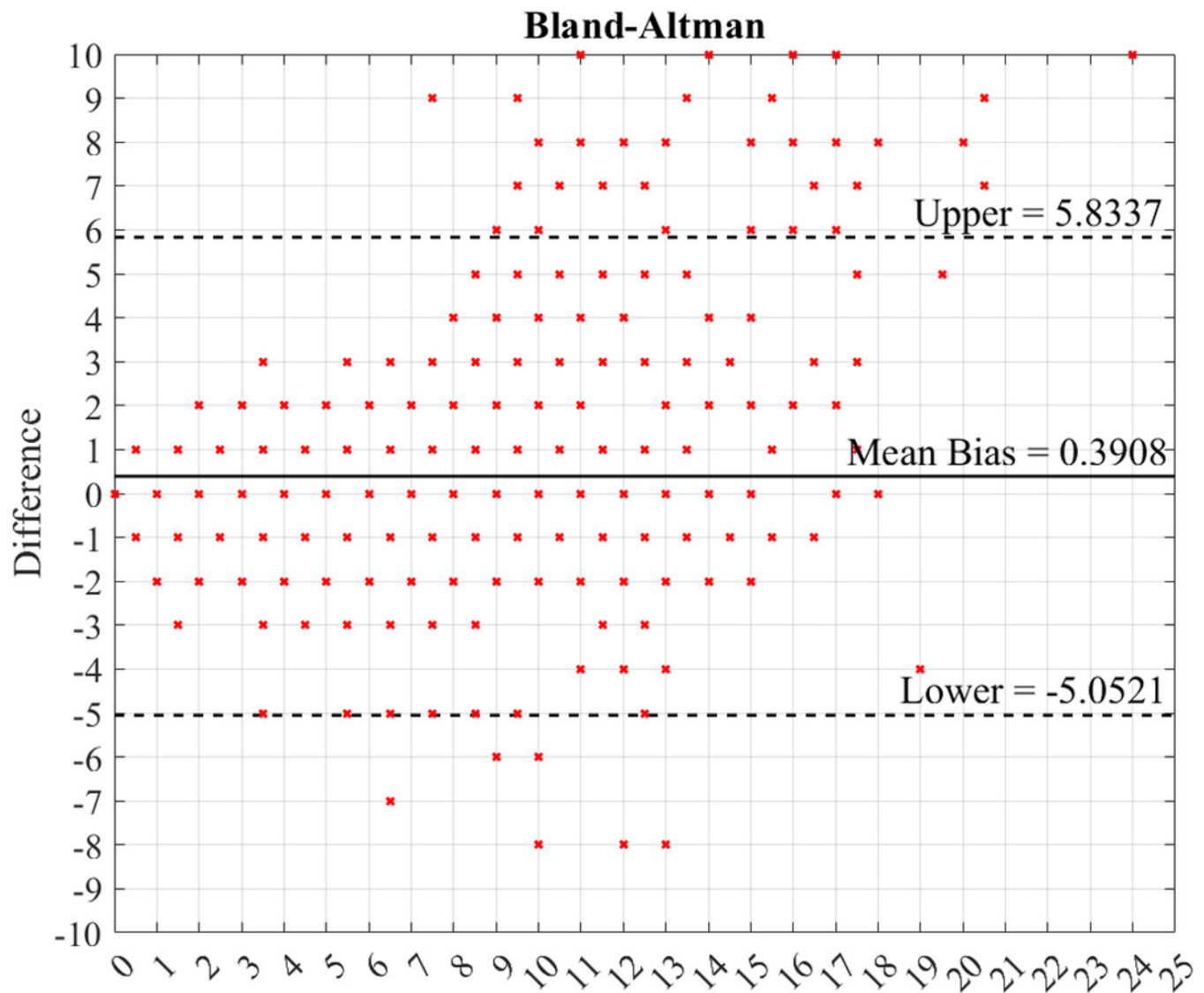
Figure 10

Fig ure 10: Distribution software error for each number of viral plaques.
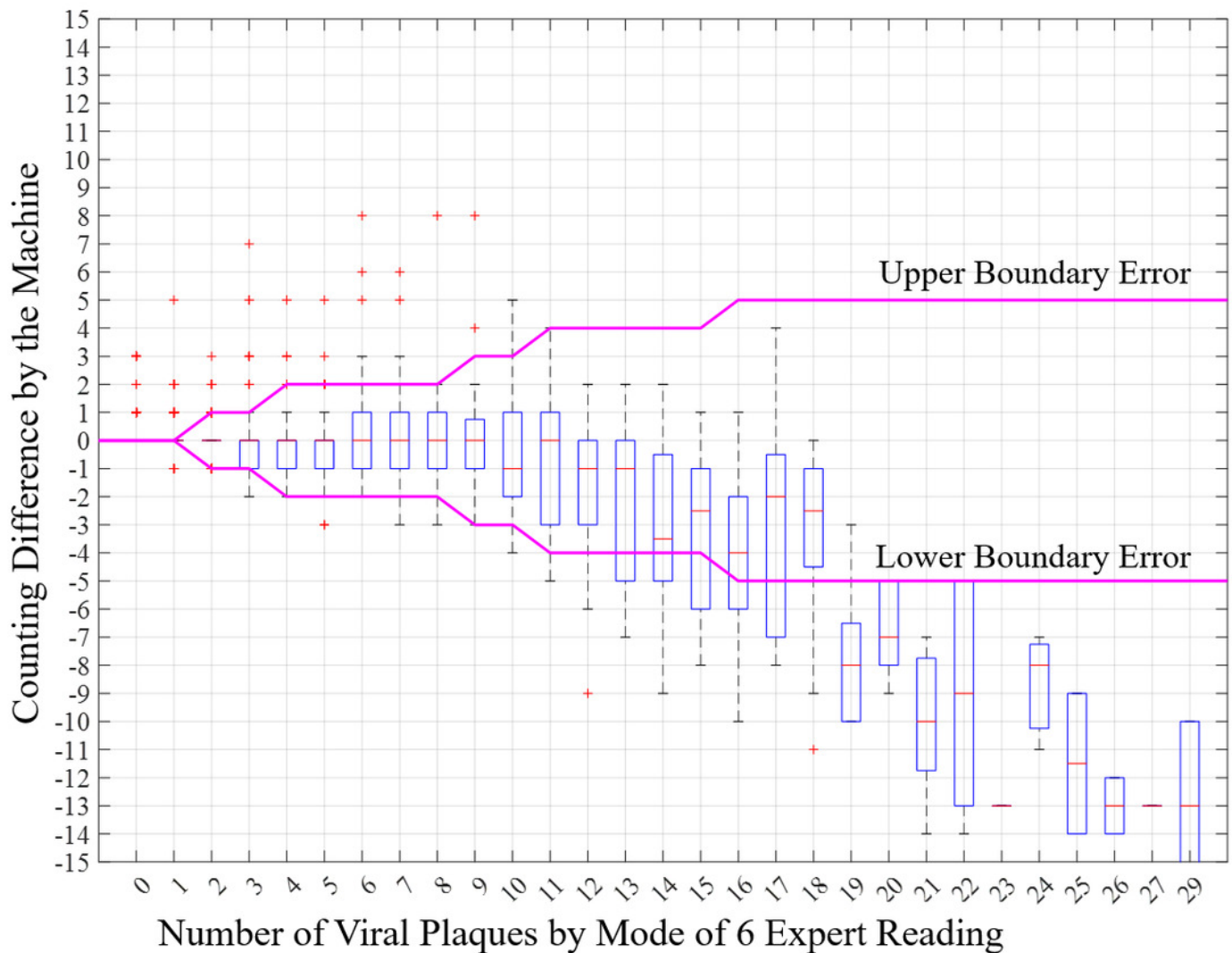
Figure 11

Figure 11: Percentage of correct measurement by the machine.